Classification: PHYSICAL SCIENCES / CHEMISTRY / PHYSICS

Relaxation dynamics of NH stretching vibrations of 2-aminopyridine and its dimer in a supersonic beam

Yuji Yamada*,[†], Naohiko Mikami[†] and Takayuki Ebata[‡,§]

*Department of Chemistry, Graduate School of Science, Tohoku University, Sendai, 980-8578, Japan

[†]Department of Chemistry, Graduate School of Science, Kobe University, Kobe, 657-8501, Japan

[‡]Department of Chemistry, Graduate School of Science, Hiroshima University, Higashi-Hiroshima, 739-8526, Japan

Corresponding author: Takayuki Ebata, Higashi-Hiroshima, 739-8526, Japan,

Tel: +81(Japan)-82-424-7407, FAX: +81(Japan)-82-424-7407,

E-mail: tebata@hiroshima-u.ac.jp

Manuscript information: Text 21 pages, Figure 7 pages, Table 2 pages.

Abbreviation:

2AP (2-aminopyridine), IVR (intramolecular vibrational energy redistribution), VP (vibrational predissociation), VER (vibrational energy relaxation), ν_s (NH_2 symmetric stretch), ν_a (NH_2 asymmetric stretch), H-bond (hydrogen-bond).

Abstract

Picosecond time-resolved IR-UV pump-probe spectroscopy has been carried out in order to elucidate vibrational energy relaxation (VER) of the NH stretching vibrations of 2-aminopyridine monomer (2AP) and dimer ($(2AP)_2$) in supersonic beams. In bare 2AP, intramolecular vibrational energy redistribution (IVR) of the NH vibrations is described by the two bath mode model, where the initial vibrational energy flows to the doorway states rapidly (6.5 ps) and then dissipates into the dense bath states with a time constant of ~20 ps. No clear difference was observed in the IVR lifetime between the symmetric and asymmetric NH_2 stretch modes. In $(2AP)_2$, IVR and vibrational predissociation (VP) were involved in VER. It was found that the rate constants of both IVR and VP of the hydrogen-bonded NH stretching vibration are larger than those of the free NH.

Vibrational energy relaxation (VER) plays a crucial role in the reactions of chemical, biological and physical systems, because the reactions initiated by the excitation of a quantum state or a specific site are accompanied by VER (1,2). Thus, VER has been well studied for several decades in condensed phase (3-7) as well as in the gas phase (7-12). In condensed phase, molecules excited to a specific vibrational level redistribute the vibrational energy very rapidly within the molecules. This process is called intramolecular vibrational energy redistribution (IVR). After IVR, the molecules experience vibrational energy transfer into the solvent molecules and intermolecular modes (6). In the gas phase, VER processes have been studied in microscopic level by using bare molecules and clusters cooled in molecular beams (13-16). For electronic excited molecules and clusters, a variety of laser spectroscopic works have been carried out for the study of VER, such as the measurements of fluorescence spectra (11,13) and time profiles of pump-probe methods (14). For the molecules in the electronic ground state, studies on VER were mostly done in frequency domain (2,8,15), and the time domain studies have not been carried out so much until very recently. In 2001, we first reported a study on IVR of the OH stretching vibration of jet-cooled phenol by picosecond IR-UV pump-probe spectroscopy (16). Since then, we have been studying VER of X-H (X = O, N, C) stretching vibrations of aromatic molecules and their clusters. In the present study, we report on VER of 2-aminopyridine (2AP) and its dimer ($(2AP)_2$) in supersonic beams.

The electronic states of 2AP have been well studied by many researchers (17-20), because of the interest in the coupling between the $\pi\pi^*$ and $n\pi^*$ states. In addition, 2AP is thought to be a simple model molecule of nucleobase, namely cytosine

(21-24). Recently Schultz and coworkers measured the lifetime of the S_1 ($\pi\pi^*$) state of 2AP clusters, and found that the lifetime of $(2AP)_2$ is remarkably short (21). They proposed that the formation of the dimer pair accelerates internal conversion of S_1, and that the same mechanism will be applicable to the short S_1 lifetime of DNA base pair.

In this study, we report on the dynamics of the NH stretching vibration of 2AP and $(2AP)_2$ in the electronic ground state. 2AP has the symmetric (ν_s, 3441 cm^{-1}) and asymmetric (ν_a, 3548 cm^{-1}) NH_2 stretching vibrations (25). We investigate the mechanism of the IVR process and determine the time scale for these two modes. As to $(2AP)_2$, there is a center of inversion symmetry, and the frequencies and motions of the NH stretching vibrations drastically change from those of monomer. $(2AP)_2$ exhibits two IR active modes, the H-bonded NH stretch (3319 cm^{-1}) and the free NH stretch (3529 cm^{-1}) (25). The large change in the vibrational frequencies should affect the IVR mechanism. These vibrational energies are higher than the H-bonding energy (2700 cm^{-1}) of $(2AP)_2$ (25). Therefore, the vibrationally excited $(2AP)_2$ can relax by vibrational predissociation (VP). Here, we apply picosecond IR-UV pump-probe spectroscopy to 2AP and $(2AP)_2$ and compare results with those of our previous work on aniline and phenol to find a general rule of VER of the X-H stretching vibration.

Picosecond IR-UV pump-probe spectroscopy is one of the most powerful tools for investigating VER of gas-phase molecules. Details of the experimental setup were described in the previous papers (16,26-30). The energy levels of 2AP and $(2AP)_2$ with the IR-UV pump-probe scheme are shown in Figs. 1*a* and 1*b*, respectively Jet-cooled 2AP and $(2AP)_2$ are generated by supersonic expansion of 2AP vapor seeded in He carrier gas through a pulsed nozzle. The free jet is skimmed, forming a molecular beam.

The molecules in the supersonic beam are excited to the NH stretching level (ν_{NH}) by a tunable picosecond IR pulse. The population of the vibrationally excited molecules is monitored by a picosecond UV pulse through 1+1 resonance enhanced multiphoton ionization (REMPI) via the S_1 state. The ions (m/Z = 94 and 188) are mass-analyzed by a 50 cm time-of-flight tube and are detected by an electron multiplier. The 1+1 REMPI spectra from the initial ν_{NH} level and doorway states {*l*} show well-resolved sharp bands, while those from dense bath states {*bath*} exhibit broad continuum due to the overlap of many transitions. Therefore, the population of ν_{NH}, {*l*} and {*bath*} can be separately observed from each other by tuning the UV laser to a proper frequency. The time profile of the population is measured by changing the delay time between the IR and the UV pulses. The tunable IR and the UV pulses were generated by the OPG/OPA systems pumped by a mode-locked picosecond Nd^{3+}:YAG laser. The bandwidth of UV light was 5 cm^{-1}, and that of the IR light was 15 - 20 cm^{-1}. The pulse widths of the pump IR and probe UV lasers were determined to be 12 ps by cross correlation measurement. The pump-probe signals were convoluted by using the time profiles of the pulses.

Results and Discussion

Analysis of pump-probe time profile of 2AP monomer

The transient 1+1 REMPI spectra observed after the IR pulse excitation to ν_s (3441 cm^{-1}) and ν_a (3548 cm^{-1}) are shown in the upper panel in Figs. 2*a* and *b*, respectively. The band origin of 2AP is located at 33466 cm^{-1} (25). The sharp bands at 30025 and 30937 cm^{-1}, which appear at short delay times in Fig. 2*a*, can be assigned to

$(\nu_s)_1^0$ and $(\nu_s)_1^0 I_0^2$, respectively, from the frequencies of the band origin and the NH vibrations. Here "I" means the inversion mode of the amino group (17). Those bands disappear rapidly with increasing the delay time. In the case of ν_a excitation (Fig. 2*b*), no sharp transition from the ν_a level, such as $(\nu_a)_1^0$, is seen at the expected position. Instead, a several peaks which cannot be assigned to the transition from the ν_s level appear when the two laser pulses are overlapped. We found that this feature is due to non-resonant ionization, which will be discussed. Missing of the $(\nu_a)_1^0$ band can be explained by the symmetry. As in the case of aniline, the NH_2 stretching vibrations are localized motions (see the vector motion in Figs. 2*a* and 2*b*). Then, ν_s and ν_a belong to a_1 and b_2 species, respectively, if we regard 2AP as a C_{2v} molecule. Then, the $(\nu_a)_1^0$ transition becomes symmetry (or Franck-Condon) forbidden. Actually, we did not observe the $(\nu_a)_1^0$ band in aniline (28). In both the REMPI spectra, broad continuum is seen at the UV frequency higher than 31800 cm^{-1} and its intensity increases with increasing the delay time. This continuum is observed in all the aromatic molecules investigated (12,26-29) and assigned to the v' – v" transitions from the redistributed states (v") generated by IVR. As will be shown later, the density of states in the region of ν_{X-H} (X = C, N, O) is more than 200 /cm^{-1}, and many transitions from the redistributed levels are overlapped and the spectrum displays the broad continuum. The reason why the v' – v" transitions appear in the lower frequency region of the band origin is that most of the vibrational frequencies decrease upon the $\pi\pi^*$ electronic excitation in aromatic molecules. Peaks marked by asterisks in the spectra are due to the irregularity of the probe UV intensity at these positions.

The time profiles obtained at several UV frequencies after the IR excitations of

ν_s and ν_a are shown in the lower panel of Fig. 2. The time profiles observed by monitoring resonant transitions from the ν_s level, $(\nu_s)_1^0$ and $(\nu_s)_1^0 I_0^2$, show rapid decay. The profiles observed by monitoring the broad continuum exhibit monotonous rise and reach a plateau at longer delay times. We first reproduce the time profiles by single exponential decay and rise functions with time constants of k_{decay} (= $1/\tau_{decay}$) and k_{rise} (= $1/\tau_{rise}$), respectively,

$$I_{NH_2}(t) = I_0 \exp(-k_{decay} t), \qquad \textbf{[1a]}$$

and

$$I_{Bath}(t) = I_0 \{1 - \exp(-k_{rise} t)\}. \qquad \textbf{[1b]}$$

The time constants obtained by the least-square fitting of the convoluted curves with the pulse duration of 12 ps are also given in the figure.

The decay rate constant of ν_s was obtained to be 1.5×10^{11} s^{-1} (= 1/6.5 ps), where we took an average of the decay time constants of $(\nu_s)_1^0$ and $(\nu_s)_1^0 I_0^2$. The time constants obtained for the rise curves are different at monitoring UV frequencies. We found that this discrepancy comes from the presence of non-resonant ion signal. Figure 3*a* shows the IR spectra observed at different delay times, where the probe UV frequency is fixed to 33270 cm^{-1}, corresponding to the broad continuum. The NH_2 stretching vibrations are clearly resolved when the delay time is fixed to 60 ps, while the broad feature appears when the delay time is zero ps. Then, we measured the time profiles of pump-probe signal with and without the IR laser frequency resonant to the NH_2 stretching vibration (Fig. 3*b*). As seen in the figure, an enhancement is seen even if the IR frequency is not resonant to the NH_2 vibrational transition. The time profile of this non-resonant signal can be reproduced as cross correlation of the two pulses, which

means that this signal occurs only when the two laser pulses are overlapped. Therefore, the pump-probe rise curve includes the non-resonant signal, and it is necessary to subtract this part from the rise curve (solid circles in Fig. 3*b*) for obtaining the true time constant. k_{rise} obtained after this subtraction is 5×10^{10} s^{-1}. We carried out the same procedure for all the pump-probe curves and obtained $k_{rise} = 3 - 5 \times 10^{10}$ s^{-1}, which is independent of the vibrational mode within the experimental error. Though the origin of this non-resonant ion signal is not clear, a possible explanation is the enhancement by UV-IR (2+1') ionization through high lying Rydberg states, whose scheme is described in Fig. 3*c*.

Mechanism of IVR: two bath mode model and prediction of doorway state

From the above analysis, we obtained k_{decay} $(= 1/\tau_{decay}) = 1.5 \times 10^{11}$ s^{-1} $(= 1/6.5$ ps) for the ν_s population decay, and k_{rise} $(= 1/\tau_{rise}) = 3 - 5 \times 10^{10}$ s^{-1} $(= 1/20$-33 ps) for the profile of broad continuum. Thus, the time constant of the population decay of the initial level is not equal to that of the population increase of the dense bath states. This discrepancy cannot be explained by one bath mode model where the IR pumped level is directly coupled with dense bath states. If it is the case, the value of k_{decay} should be equal to that of k_{rise}. This disagreement was also observed in aniline (28). Thus, in aniline and 2AP, IVR of the high frequency vibrational modes is described by two bath mode model instead of the one bath mode model (Fig. 1*a*). In the two bath mode model, the vibrational energy put to the IR active level initially flows into the specific states $\{l\}$ called doorway states (31,32), (first IVR), with the rate constant of k_1 $(= 1/\tau_1)$. The energy further dissipates to the dense bath states (second IVR), $\{bath\}$, with a rate

constant of k_2 (= $1/\tau_2$). The validity of the two bath mode model was suggested in our previous studies on IVR of OH stretch of phenol (26) and NH_2 stretch of aniline (28,29). Actually, in the case of the IVR of the OD stretching vibration of phenol-d_1, we directly observed the doorway state (27).

In the two bath mode model, the time profile of the initial state is expressed as follows,

$$I_{NH_2}(t, \nu_{UV}) = A(\nu_{UV})\, I_0 \exp(-k_1 t), \qquad \textbf{[2a]}$$

where I_0 means the initial population excited to the ν_s level and $A(\nu_{UV})$ is the frequency dependent intensity factor. The time profiles of the doorway states, $I_{Doorway}(t, \nu_{UV})$, and the dense bath states, $I_{Bath}(t, \nu_{UV})$, are,

$$I_{Doorway}(t, \nu_{UV}) = B(\nu_{UV})\, I_0 \frac{k_1}{k_1 - k_2} \{\exp(-k_2 t) - \exp(-k_1 t)\}, \qquad \textbf{[2b]}$$

and

$$I_{Bath}(t, \nu_{UV}) = C(\nu_{UV})\, I_0 \left[1 + \frac{k_2}{k_1 - k_2}\exp(-k_1 t) - \frac{k_1}{k_1 - k_2}\exp(-k_2 t)\right]. \qquad \textbf{[2c]}$$

The rate constant of the first step (k_1) is directly determined to be 1.5×10^{11} s^{-1} (= 1/6.5 ps). The transition from the doorway state is expected to give sharp bands in the transient REMPI spectra, and its time profile exhibits the rise and the decay expressed by Eq. 2*b*. However, we cannot see any sharp transitions attributable to the doorway states in the transient REMPI spectra of Figs. 1*a* and 1*b*, so their intensities are thought to be very weak and overlapped with the broad continuum. Thus, we reproduced the time profile of the broad continuum after exciting ν_s by the superposition of the curves expressed by Eqs. 2*b* and 2*c*, and the result is shown as the thick solid curve in Fig. 4. Here, thin solid curves correspond to the time profiles of Eqs. 2*b* and 2*c*, respectively.

We obtained $k_2 = 4.3 \times 10^{10}$ s^{-1} (= 1/23 ps) by least-square fitting procedure. Though this curve fitting by using Eq. 2*c* gives the best result, we found that even a simple fitting by using a single exponential rise function gives a reasonable result. That is, we obtained k_2 (= k_{rise}) = 4.5×10^{10} s^{-1} (= 1/22 ps) by the fitting with Eq. 1*b*. This value is good enough by taking account of the uncertainty of the obtained values ($\pm$15%). The result indicates that the contribution of $I_{Doorway}(t, \nu_{UV})$ and second term in Eq. 2*c* to the broad continuum is very small. The rate constants obtained for the first and the second IVR process are listed in Table 1. We also carried out similar analysis for ν_a. In this case, we could not obtain k_1, and only k_2 value is listed. We do not have a clear explanation why we could not observe the UV transitions from the doorway states. A possible explanation is that those transitions have very small Franck-Condon activity in the region observed in the present study.

Comparison with IVR of other system

In Table 1, the rate constants obtained for 2AP are compared with those of the NH_2 stretch of aniline (28) and the OH stretch of phenol (26). Also listed is the density of states, ρ, in the energy region of these vibrations. For phenol and aniline, the values of ρ were given in previous papers (26,28). For 2AP, we calculated ρ by direct counting method using the fundamental frequencies obtained by the density functional theory (DFT) method at the B3LYP/cc-pVTZ level with Gaussian 03 package (33). We used a scaling factor of 0.9627 to reproduce the frequencies of ν_s and ν_a. In the table, we first see that the value of k_1 for ν_s of 2AP is 2.7 times larger that that of aniline. Since the values of ρ are not so different between them, this difference is explained by the larger

"$\nu_s \leftrightarrow$ doorway state" anharmonic coupling of 2AP than that of aniline. Another noticeable point is that k_2 is smaller than k_1, in 2AP, and the same tendency is seen in aniline, although the value of k_2 has large uncertainty. Interestingly, this situation is quite different from the phenolic OH stretching vibration, that is k_2 is much larger than k_1. We consider that this difference is attributed to the characters of the doorway states. In our previous works, we reported that the doorway state involves the CH stretch vibrations in the IVR of phenolic OH stretch (26). On the other hand, the CH mode does not play a part in IVR of the NH_2 stretch of aniline (29). In addition, it is well known that the CH stretch is strongly coupled with the combination of the lower frequency modes by Fermi resonance. This coupling controls rapid energy redistribution in the second step of the IVR process. Thus, we conclude that the existence or nonexistence of the CH stretching vibration in the doorway states leads to a large difference in the second IVR rate.

Analysis of pump-probe time profiles for $(2AP)_2$

The electronic spectrum and the IR spectra of $(2AP)_2$ were already investigated by Brutschy and coworkers (25). The band origin of $(2AP)_2$ is located at 31805 cm^{-1}, which is 1661 cm^{-1} red-shifted from the monomer band origin. $(2AP)_2$ exhibits the H-bonded NH stretch at 3319 cm^{-1} and the free NH stretch at 3529 cm^{-1}. The binding energy of $(2AP)_2$ is estimated to be 2700 cm^{-1} (25), so the vibrationally excited dimer can dissociate via vibrational predissociation (VP). Figures 5*a* and 5*b* show the transient 1+1 REMPI spectra of $(2AP)_2$ observed after the excitation to the H-bonded NH and the free NH stretching vibrations, respectively. In both cases, broad continuum due to

transitions from redistributed levels appears in the region lower than the dimer origin band at 31805 cm^{-1}. Different from bare 2AP, the broad continuum disappears with increasing the delay time due to VP. In $(2AP)_2$, we could not observe the resonant transition from the NH stretch vibrational level, such as the $(\nu_{NH})_1^0$ band. This is due to the symmetrical reason. $(2AP)_2$ belongs to C_i point group, and the dipole allowed S_1 state is ^1A_u. As to the symmetric species of the vibrational level, the IR active NH stretching vibrational level belongs to a_u, and the zero-point vibrational level of S_1 belongs to a_g. Thus, the Franck-Condon factor of the $(\nu_{NH})_1^0$ transition is zero.

Though we cannot observe the decay of the NH stretch level, we can investigate IVR and VP of $(2AP)_2$ by analyzing the time profile of the broad continuum corresponding to population of dense bath states shown in Fig. 6. The time profiles were independent of the probe UV frequencies. For analyzing the times profiles of $(2AP)_2$, we used two-step VER model (Fig. 1*b*). As was discussed above, in bare 2AP, the time constant $k_{rise} = 4.5 \times 10^{10}$ s^{-1} obtained by Eq. 1*b* is almost equal to $k_2 = 4.3 \times 10^{10}$ s^{-1} obtained by two bath mode model. This is because k_1 is much faster than k_2. In addition, we reported that the first IVR step (k_1) is substantially accelerated by H-bonding (30). This means that in $(2AP)_2$ the first IVR process ($\nu_{NH} \rightarrow$ doorway state) is too fast to be observed with our laser pulse width (12 ps), and the rate determining step of IVR will be the "doorway state $\rightarrow$ dense bath state" process.

Thus, we used the two-step VER model, the first step is the "$\nu_{NH} \rightarrow$ dense bath state" with a rate constant k_2 and the second step is "dense bath state $\rightarrow$ dissociation continuum" (VP) with a rate constant k_{VP}. Thus, we carried out the least-square fitting by using the following equation,

$$I_{continuum}(t) = I_0 \frac{k_2}{k_2 - k_{VP}} \{ \exp(-k_{VP} t) - \exp(-k_2 t) \}. \quad \textbf{[3]}$$

Another noticeable point in Fig. 6 is that each curve does not completely reach to zero at longer delay time due to unavoidable fragmentation from higher clusters after the ionization. We reproduced this nonzero baseline by a step function, assuming that the fragmentation of higher cluster is very fast. The time constants obtained are listed in Table 2.

Effect of the formation of H-bond on IVR

As seen in Table 2, k_2 is larger by a factor of more than five in the H-bonded NH stretch and by a factor of two in the free NH stretch than that of bare 2AP. Thus, the IVR process is greatly accelerated by the H-bonding. This acceleration can be explained by the increase of the anharmonic coupling and the state density of the bath mode (6). Then, we examined the latter effect by the direct counting of the vibrational levels of $(2AP)_2$. The vibrational frequencies were obtained by the DFT calculation (B3LYP/cc-pVTZ level). Here, we used the same scaling factor as that of monomer (0.9627), resulting in a frequency of 3542 cm^{-1} for the free NH stretch and 3221 cm^{-1} for the H-bonded NH one. Thus, the agreement between the calculated and the observed frequency (3319 cm^{-1}) is not so good for the H-bonded NH stretch due to the large anharmonicity (34). In spite of the disagreement, the present calculation is good enough for the qualitative examination of the effect of state density. For the state density calculation, we took into account a symmetry restriction for IVR, since the matrix element of anharmonic coupling is nonzero only between the states with the same species. The state density obtained by the direct counting is 1.63×10^8 and $3.63 \times$

10^8 /cm^{-1} at the H-bonded and the free NH stretch, respectively. Thus, the state density of dimer is roughly 10^6 times larger than monomer. On the other hand, the observed enhancement is a factor of five for the H-bonded NH stretch and two for the free NH one. The result indicates that the coupled levels which control the IVR rate are very much limited and the total density of states is not so important. This conclusion is also supported by the fact that the state density at the free NH stretch region is larger than that of the H-bonded NH one, which is opposite to the observed k_2.

Mode dependence of the VP rates

Finally, we discuss VP rate constants of $(2AP)_2$. From the decay profile of the broad continuum, we obtained $k_{VP} = 3.6 \times 10^{10}$ s^{-1} for the H-bonded NH stretch and $k_{VP} = 2.5 \times 10^{10}$ s^{-1} for the free NH one. These results are compared with those predicted by RRKM theory (35) to examine whether VP occurs statistically or not. In this theory, the dissociation rate constant is given by the following equation,

$$k_{RRKM}(E) = G^*(E - D_0)/h\rho(E), \qquad \textbf{[3]}$$

where $\rho(E)$ is the density of states of the dimer at the total energy of E, and $G^*(E - D_0)$ is the number of possible states of fragments at an available energy of $E - D_0$. D_0 is the binding energy; we adopted the reported value of 2700 cm^{-1} (25). The calculated VP rate constant of $(2AP)_2$, k_{RRKM}, as a function of the excitation energy is shown in Fig. 7. The k_{RRKM} curve monotonously increases with the excitation energy. Since the energy of the free NH stretch is larger than the H-bonded NH stretch, one can immediately predict that k_{RRKM} of the free NH stretch is larger than the H-bonded one. Actually, the values of k_{RRKM} are obtained 1.1×10^6 and 2.9×10^6 s^{-1} for H-bonded and free NH

stretch, respectively. The absolute values of the calculated k_{RRKM} are four orders of magnitudes smaller than the experimental data. Moreover, the calculated result cannot reproduce even the order of the observed VP rate constant for the free and the H-bonded NH stretches.

Such a disagreement between the VP rate constants observed and estimated by statistical theory has been reported by several systems (36-38). In $(HF)_2$, for example, the VP lifetime of the H-bonded HF stretch (3868 cm^{-1}) is 0.48 ns, while that of the higher frequency free HF stretch (3929 cm^{-1}) is 20 ns (36,37). In the $(HF)_2$ case, the vibrational state density is very low, and the VP rate constant was estimated quantum mehcanically by considering the overlap integral of the initial vibrational wavefunction and the translational wavefunction of fragments (39-41). With the increase of the excess energy, the overlap integral between the vibrational and the translational wavefunctions becomes small, resulting in a smaller VP rate constant for energetically higher free HF stretch vibration. Ewing suggested that the VP lifetime is proportional to the translational momentum of fragments, called the momentum-gap correlation (41). It is not clear whether this momentum-gap correlation can be applied to VP of $(2AP)_2$ because of the complexity of the cluster and the existence of IVR. However, it should be also noted that the larger VP rate constant of the H-bonded OH stretch than that of the free one was also observed in the phenol dimer (16). Thus, this tendency seems to be a common feature. Another possibility is that IVR is not completed before VP and the H-bonded X-H (X = F, O and N) stretch has some special route leading to the dissociation channel.

Conclusions

In this article, picosecond time-resolved IR-UV pump-probe spectroscopy has revealed the VER mechanism of the NH_2 stretching vibrations of jet-cooled 2AP monomer and dimer in the S_0 state. IVR of the NH_2 stretch of 2AP is described by the two bath mode model. This mechanism was also observed for other systems, such as phenolic OH stretch and the NH_2 stretch of aniline. However, the time scale of each IVR step is quite different for different systems, which may depend on the character of the doorway states. Of particular importance is that whether the doorway state involves the CH stretching vibration or not leads to a large difference in the second step IVR rate; the second step IVR is very fast in phenolic OH stretch, where CH stretch is involved in the doorways state. On the other hand, the second step is relatively slow in aniline and 2AP, where CH stretch is not involved in the doorways state.

In $(2AP)_2$, the observed enhancement of IVR by the H-bond formation is much smaller than that expected from the increase of the density of states, indicating an importance of anharmonic coupling. The H-bonded NH stretching vibration exhibits larger IVR and VP rate constants than those of the free NH stretch. The mode dependence of IVR can be described by the larger "NH stretching vibration ↔ bath states" anharmonic coupling of the former mode than the latter. For VP, a simple statistical theory cannot explain the observed mode dependence of the rate constant, and other approaches, such as quantum theoretical or non-statistical treatment, are suggested.

ACKNOWLEDGMENT

This work is supported by the Grant-in-aids for Scientific Research (Grant 18205003) by JSPS. One of the authors (Y.Y.) thanks the support from COE project of Tohoku University. Another author (N.M.) acknowledges the support for Grant-in-Aids for specially promoted Research (Grant No. 16002006) by MEXT.

Footnotes

[§]To whom correspondence should be addressed at: Department of Chemistry, Graduate School of Science, Hiroshima University, Higashi-Hiroshima, 739-8526, Japan. E-mail: tebata@hiroshima-u.ac.jp

Author contributions: Y.Y., N.M. and T.E. designed research; Y.Y. performed research and analyzed data; and Y.Y. and T.E. wrote the paper.

The authors declare no conflict of interest.

Reference

1. Owrutsky JC, Raftery D, Hochstrasser RM (1994) Vibrational relaxation dynamics in solutions. *Annu Rev Phys Chem* 45: 519-555.
2. Nesbitt DJ, Field RW (1996) Vibrational energy flow in highly excited molecules: Role of intramolecular vibrational redistribution. *J Phys Chem* 100: 12735-12756.
3. Elsaesser T, Kaiser W (1991) Vibrational and vibronic relaxation of large polyatomic molecules in liquids. *Annu Rev Phys Chem* 42: 83-107.
4. Wang Z, Pakoulev A, Dlott DD (2002) Watching vibrational energy transfer in liquids with atomic spatial resolution. *Science* 296: 2201-2203.
5. Stratt RM, Maroncelli M (1996) Nonreactive dynamics in solution: The emerging molecular view of

solvation dynamics and vibrational relaxation. *J Phys Chem* 100: 12981-12996.

6. Kenkre VM, Tokumakoff A, Fayer MD (1994) Theory of vibrational relaxation of polyatomic molecules in liquids. *J Chem Phys* 101: 10618-10629.
7. Elles CG, Crim FF (2006) Connecting chemical dynamics in gases and liquids. *Annu Rev Phys Chem* 57: 273-302.
8. Lehmann KK, Scoles G, Pate BH (1994) Intramolecular dynamics from eigenstate-resolved Infrared spectra. *Annu Rev Phys Chem* 45: 241-274.
9. Felker PM, Zewail AH (1995) in *Jet Spectroscopy and Molecular Dynamics*, eds Hollas JM, Phillips D (Blackie Academic, London), pp. 222-308.
10. Stromberg C, Meyers DJ, Fayer MD (2002) Vibrational dynamics of large hot molecules in the collisionless gas phase. *J Chem Phys* 116: 3540-3553.
11. Parmenter CS (1983) Introductory lecture. Vibrational redistribution within excited electronic states of polyatomic molecules. *Faraday Discuss Chem Soc* 75: 7-22.
12. Yamada Y, Katsumoto Y, Ebata T (2007) Picosecond IR-UV pump–probe spectroscopic study on the vibrational energy flow in isolated molecules and clusters. *Phys Chem Chem Phys* 9: 1170-1185.
13. Kelley DF, Bernstein ER (1986) An RRKM approach to vibrational predissociation of van der Waals clusters. *J Phys Chem* 90: 5164-5168.
14. Knee JL, Khundkar LR, Zewail AH (1987) Picosecond photofragment spectroscopy. III. Vibrational predissociation of van der Waals' clusters. *J Chem Phys* 87: 115-127.
15. Miller RE (1986) Infrared laser photodissociation and spectroscopy of van der Waals molecules. *J Phys Chem* 90: 3301-3313.
16. Ebata T, Kayano M, Sato S, Mikami N (2001) Picosecond IR-UV pump–probe spectroscopy. IVR of OH stretching vibration of phenol and phenol dimer. *J Phys Chem A* 105: 8623-8628.

17. Hollas JM, Kirby GH, Wright RA (1970) Electronic assignment as $^1A'(\pi\pi^*)$-$^1A'$ of the 2980 Å system of 2-aminopyridine by rotational band contour analysis. *Mol Phys* 18: 327-335.

18. Hollas JM, Musa H, Ridley T (1984) The $\tilde{A}^1A' - \tilde{X}^1A'$ absorption and single vibronic level fluorescence spectra of 2-aminopyridine. *J Mol Spectrosc* 104: 89-106.

19. Hager JW, Wallace SC (1985) Solvation effects in jet-cooled 2-aminopyridine clusters: excited-state dynamics and two-color threshold photoionization spectroscopy. *J Phys Chem* 89: 3833-3841.

20. Kydd RA (1979) The amino inversion vibration in aminopyridines. *Spectrochim Acta Part A* 35: 409-413.

21. Schultz T, Samoylova E, Radloff W, Hertel IV, Sovolewski AL, Domcke W (2004) Efficient deactivation of a model base pair via excited-state hydrogen transfer. *Science* 306: 1765-1768.

22. Frey JA, Müller A, Frey H-M, Leutwyler S (2004) Infrared depletion spectra of 2-aminopyridine·2-pyridone, a Watson–Crick mimic of adenine·uracil. *J Chem Phys* 121: 8237-8245.

23. Hager JW, Leach GW, Demmer DR, Wallace SC (1987) Structure and excited-state dynamics of 2-aminopyridine van der Waals molecules and hydrogen-bonded complexes. *J Phys Chem* 91: 3750-3758.

24. Woutersen S, Cristalli G (2004) Strong enhancement of vibrational relaxation by Watson-Crick base pairing. *J Chem Phys* 121: 5381-5386.

25. Wu R, Brutschy B (2004) Infrared depletion spectroscopy and structure of the 2-aminopyridine dimer. *J Phys Chem A* 108: 9715-9720.

26. Yamada Y, Kayano M, Ebata T, Mikami N (2004) Picosecond IR–UV pump–probe spectroscopic study of the dynamics of the vibrational relaxation of jet-cooled phenol. I. Intramolecular vibrational energy redistribution of the OH and CH stretching vibrations of bare phenol. *J Chem Phys* 120: 7400-7409.

27. Yamada Y, Mikami N, Ebata T (2004) Real-time detection of doorway states in the intramolecular vibrational energy redistribution of the OH/OD stretch vibration of phenol. *J Chem Phys* 121: 11530-11534.

28. Yamada Y, Okano J, Mikami N, Ebata T (2005) Picosecond IR-UV pump-probe spectroscopic study on the intramolecular vibrational energy redistribution of NH_2 and CH stretching vibrations of jet-cooled aniline. *J Chem Phys* 123: 124316.

29. Yamada Y, Okano J, Mikami N, Ebata T (2006) Picosecond time-resolved study on the intramolecular vibrational energy redistribution of NH stretching vibration of jet-cooled aniline and its isotopomer. *Chem Phys Lett* 432: 421-425.

30. Kayano M, Ebata T, Yamada Y, Mikami N (2004) Picosecond IR–UV pump–probe spectroscopic study of the dynamics of the vibrational relaxation of jet-cooled phenol. II. Intracluster vibrational energy redistribution of the OH stretching vibration of hydrogen-bonded clusters. *J Chem Phys* 120: 7410-7417.

31. Heller DF, Mukamel S (1979) Theory of vibrational overtone line shapes of polyatomic molecules. *J Chem Phys* 70: 463-472.

32. Hutchinson JS, Reinhardt WP, Hynes JT (1983) Nonlinear resonances and vibrational energy flow in model hydrocarbon chains. *J Chem Phys* 79: 4247-4260.

33. Frisch MJ, Trucks GW, Schlegel HB, *et al.* (2003) *Gaussian03*, (Gaussian Inc., Pittsburgh PA,) Revision B.05.

34. Lucas B, Lecomte F, Reimann B, Barth H-D, Grégoire G, Bouteiller Y, Schermann J-P, Desfrançois C (2004) A new infrared spectroscopy technique for structural studies of mass-selected neutral polar complexes without chromophore. *Phys Chem Chem Phys* 6: 2600-2604.

35. Marcus RA (1986) Product quantum state distributions in unimolecular reactions involving highly

flexible transition states. *J Chem Phys* 85: 5035-5040.

36. Pine AS, Lafferty WJ (1983) Rotational structure and vibrational predissociation in the HF stretching bands of the HF dimer. *J Chem Phys* 78: 2154-2162.
37. Nesbitt DJ (1994) High-resolution, direct infrared laser absorption spectroscopy in slit supersonic jets: Intermolecular forces and unimolecular vibrational dynamics in clusters. *Annu Rev Phys Chem* 45: 367-399.
38. Huang ZS, Miller RE (1989) High-resolution near-infrared spectroscopy of water dimer. *J Chem Phys* 91: 6613-6631.
39. Staib A, Hynes JT (1993) Vibrational predissociation in hydrogen-bonded OH…O complexes via OH stretch-OO stretch energy transfer. *Chem Phys Lett* 204: 197-205.
40. Beswick JA, Jortner J (1981) Intermolecular and intramolecular $V \rightarrow V$ transfer in the vibrational predissociation of some polyatomic van der Waals molecules. *J Chem Phys* 74: 6725-6733.
41. Ewing GE (1982) Relaxation channels of vibrationally excited Van der Waals molecules. *Faraday Discuss Chem Soc* 73: 325-33

Table 1. Rate constants ($\times$ 10^{10} s^{-1}) of each relaxation step of 2-aminopyridine, aniline and phenol.

	2AP		Aniline *		Phenol †
Frequency (cm^{-1})	ν_s (3441)	ν_a (3548)	ν_s (3423)	ν_a (3509)	ν_{OH} (3657)
k_1	15 ± 3	--	5.6	2.9	7.1
k_2	4.3 ± 0.6	4.2 ± 0.6	$0.1 < k_2 < 5$	$0.1 < k_2 < 2$	$k_1 << k_2$
ρ (/cm^{-1})	204	244	185 ‡	257 §	110 ‡

* Ref. 27.

† Ref. 26.

‡ Only the states with a' species are counted.

§ Only the states with a" species are counted.

Table 2. Rate constants ($\times$ 10^{10} s^{-1}) of each step of 2AP and $(2AP)_2$.

	2AP		$(2AP)_2$	
	ν_s(3441 cm^{-1})	ν_a (3548 cm^{-1})	H-bonded (3319 cm^{-1})	Free (3529 cm^{-1})
k_1	15 ± 3	--	--	--
k_2	4.3 ± 0.6	4.2 ± 0.6	>>20	7.7 ± 1.6
k_{VP}			3.6 ± 0.6	2.5 ± 0.3

Figure Captions

Fig. 1. (a) IR spectrum of the NH_2 stretching vibration, the energy levels and the IR pump - UV probe scheme for 2AP. {*l*} and {*bath*} are the doorway states and dense bath states, respectively. (b) The energy levels and the IR pump - UV probe scheme for $(2AP)_2$. {*bath*} and {*Diss. Cont.*} are the dense bath states and dissociation continuum, respectively.

Fig. 2. (a) (Upper) Transient 1+1 REMPI spectra of 2AP measured after the IR excitation of the NH_2 symmetric stretching vibration. (Lower) Time profiles of the transient 1+1 REMPI signals measured at several UV frequencies. (b) (Upper) Transient 1+1 REMPI spectra of 2AP measured after the IR excitation of the NH_2 asymmetric stretching vibration. (Lower) Time profiles of the transient 1+1 REMPI signals measured at several UV frequencies. The vibrational motion of each normal mode is shown in the figure. Peaks marked by asterisks are due to irregular SHG intensities at these positions. The solid curves are convoluted ones by using Eqs. 1*a* and 1*b*. See text.

Fig. 3. (a) Time-resolved IR spectra obtained at ν_{UV} = 33270 cm^{-1} at different delay times. (b) Time profiles of ion signal monitored at ν_{UV} = 33270 cm^{-1} with the pump IR frequencies fixed to the NH_2 symmetric stretch (open circles) and 3373 cm^{-1} (diamonds). Solid circles were the corrected time profile obtained by subtracting the time profile of diamonds from that of open circles. The solid curve is the least-square fitted rise function with rate constant of 5.0×10^{10} s^{-1}. (c) Proposed excitation scheme to explain non-resonant background.

Fig. 4. Time profile fitted by using superposition of Eqs. 2*b* and 2*c*. The solid thin

curves correspond to each component. The fitted parameters of k_1 and k_2 are 1.4×10^{11} and 4.3×10^{10} s^{-1}, respectively.

Fig. 5. Transient 1+1 REMPI spectra of $(2AP)_2$ measured after the IR excitation of (a) the H-bonded NH stretching vibration and (b) the free NH stretching vibration. The vibrational motion of each normal mode is also shown.

Fig. 6. Time evolutions of the transient broad continuum at several UV frequencies after exciting (a) the H-bonded NH stretching and (b) the free NH asymmetric stretching vibrations of 2-aminopyridine dimer. The solid curves are the convoluted ones by using the rate constants listed in Table 2.

Fig. 7. Plot of VP rate constant of $(2AP)_2$ calculated by RRKM theory as a function of excitation energy. The dissociation threshold is assumed to be 2700 cm^{-1} and arrows in figure indicate the NH stretching bands excited in our experiment.

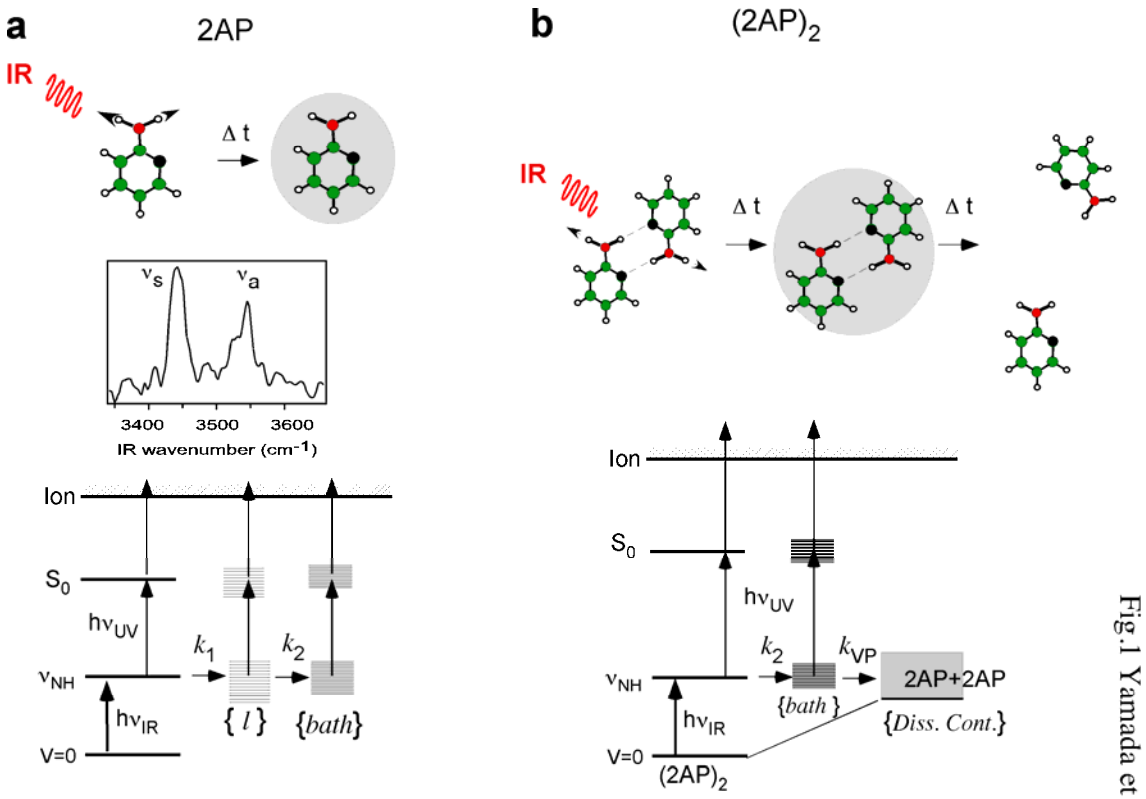

Fig.1 Yamada et al.

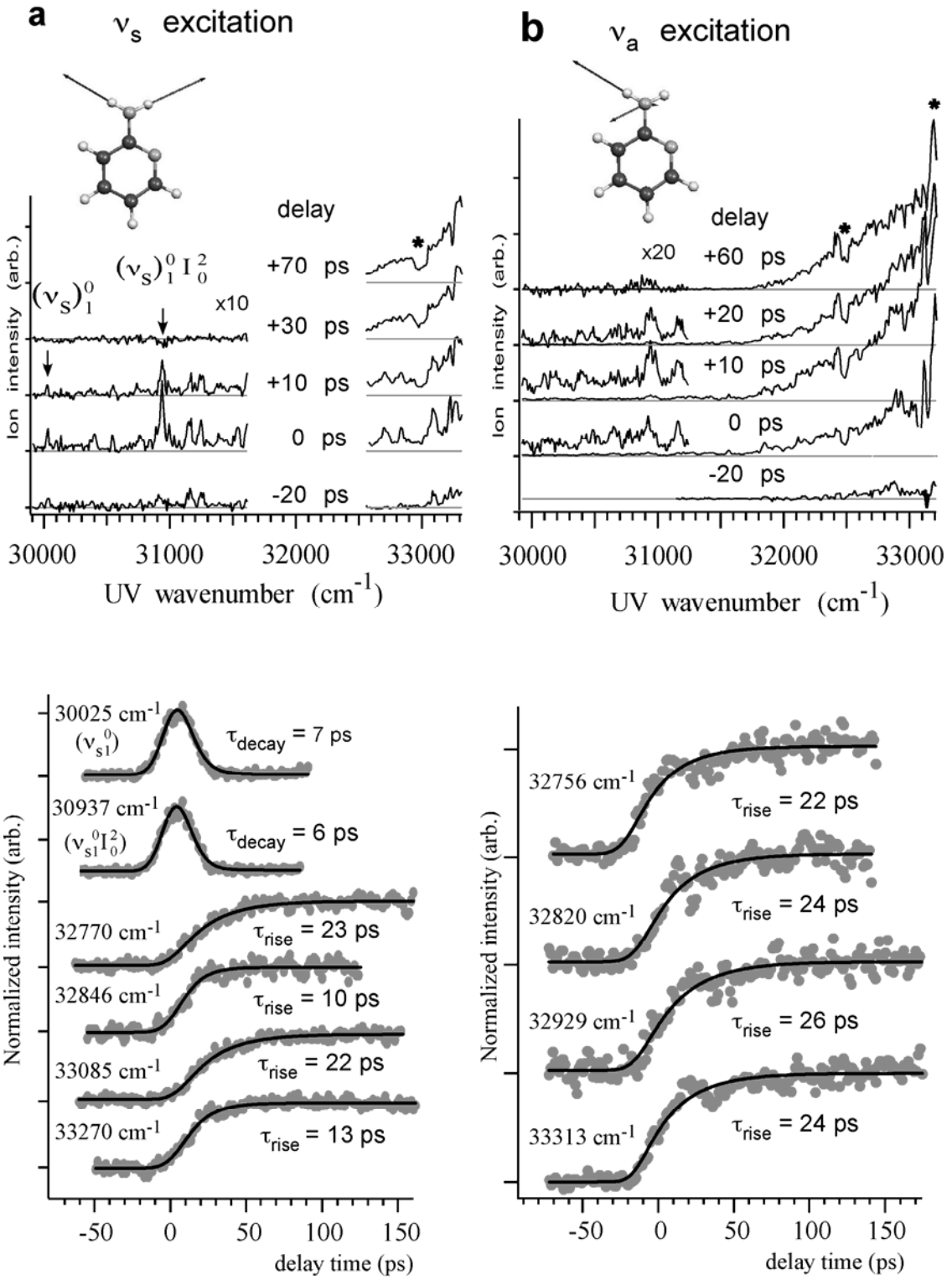
a
ν_s excitation
delay
$(\nu_S)_1^0 I_0^2$
$(\nu_S)_1^0$
x10
+70 ps
+30 ps
+10 ps
0 ps
-20 ps
Ion intensity (arb.)
30000
31000
32000
33000
UV wavenumber (cm^{-1})
b
ν_a excitation
delay
x20
+60 ps
+20 ps
+10 ps
0 ps
-20 ps
Ion intensity (arb.)
30000
31000
32000
33000
UV wavenumber (cm^{-1})
30025 cm^{-1}
(ν_{s1}^0)
τ_{decay} = 7 ps
30937 cm^{-1}
$(\nu_{s1}^0 I_0^2)$
τ_{decay} = 6 ps
32770 cm^{-1}
τ_{rise} = 23 ps
32846 cm^{-1}
τ_{rise} = 10 ps
33085 cm^{-1}
τ_{rise} = 22 ps
33270 cm^{-1}
τ_{rise} = 13 ps
Normalized intensity (arb.)
-50
0
50
100
150
delay time (ps)
32756 cm^{-1}
τ_{rise} = 22 ps
32820 cm^{-1}
τ_{rise} = 24 ps
32929 cm^{-1}
τ_{rise} = 26 ps
33313 cm^{-1}
τ_{rise} = 24 ps
Normalized intensity (arb.)
-50
0
50
100
150
delay time (ps)

Fig. 3 Yamada et al.

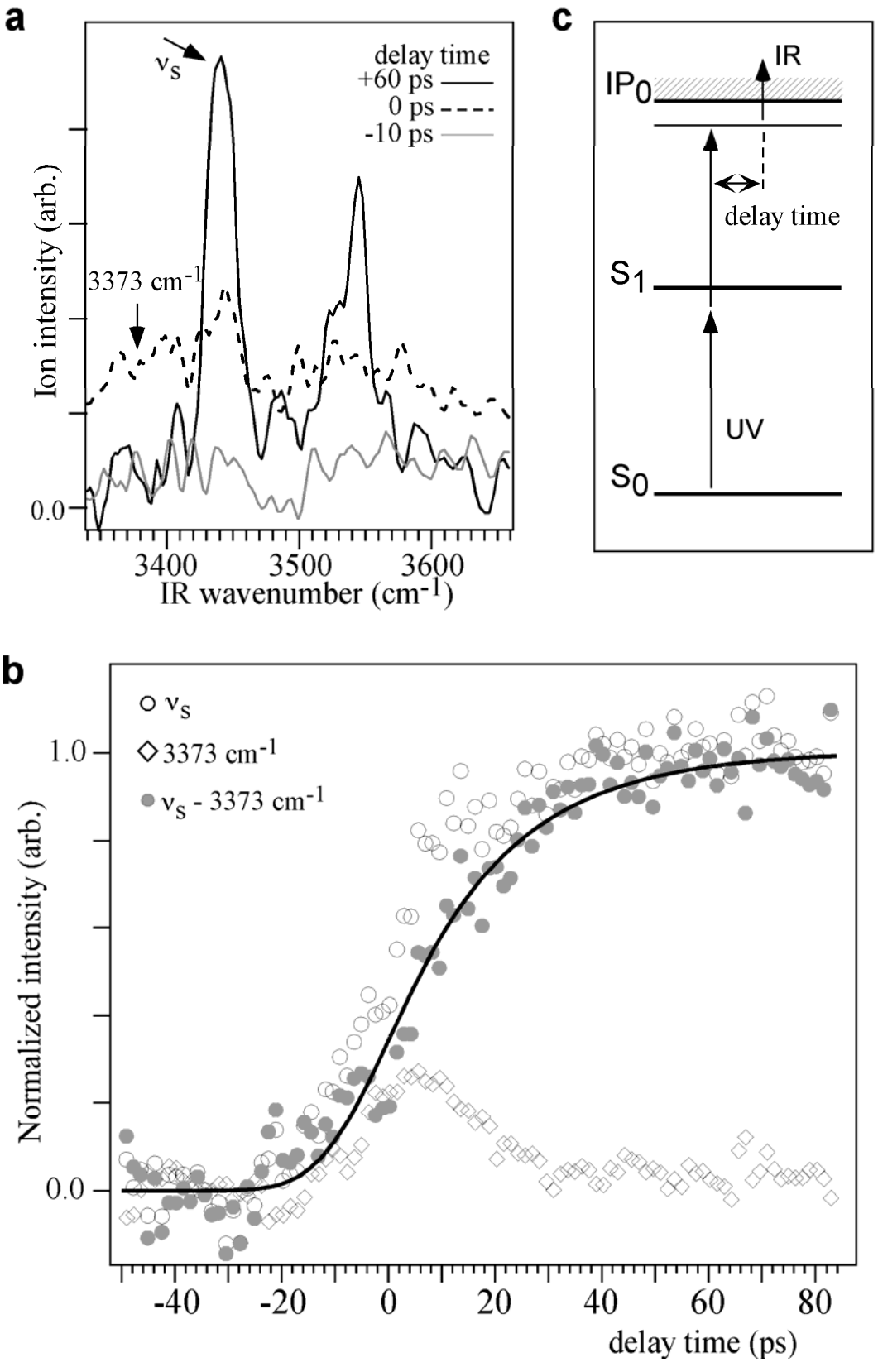

Fig. 4 Yamada et al.

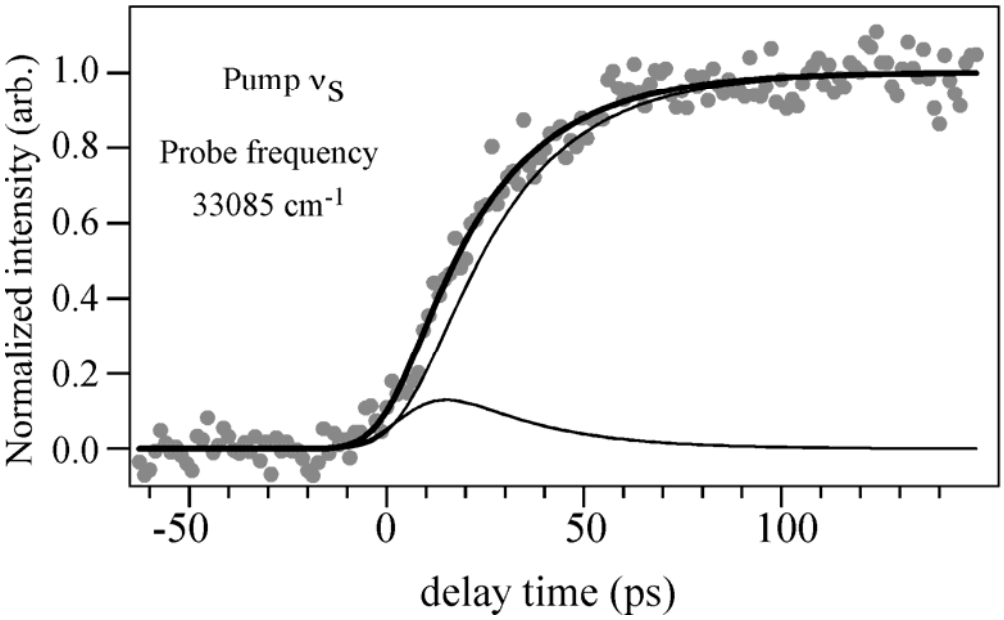

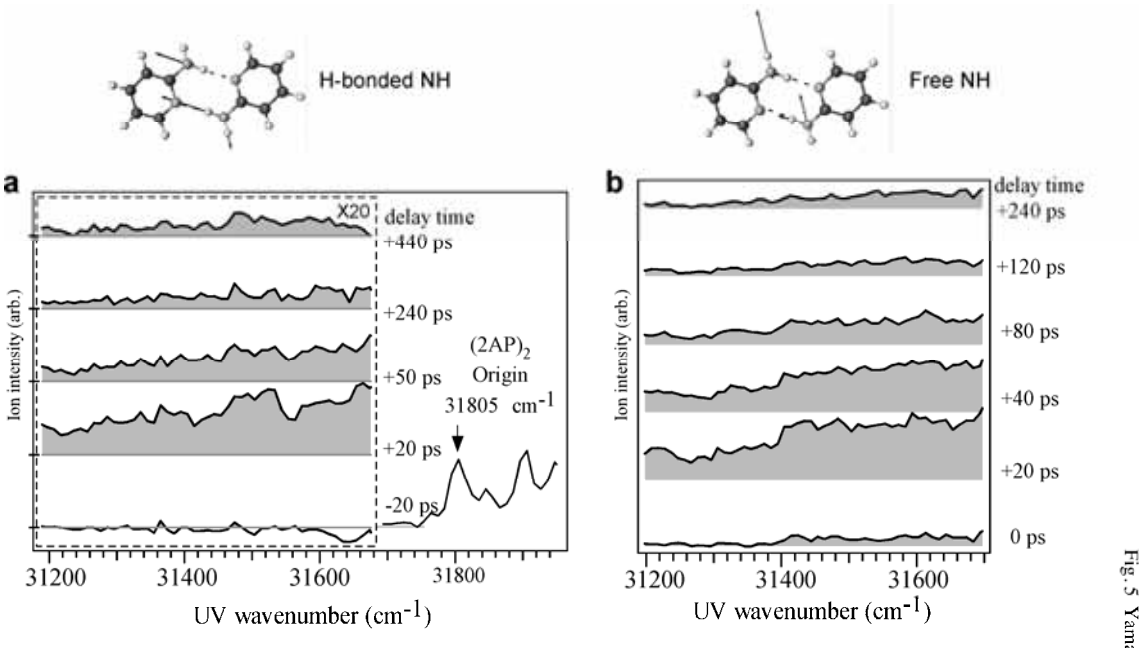

Fig. 5 Yamada et al.

Fig.6 Yamada et al.

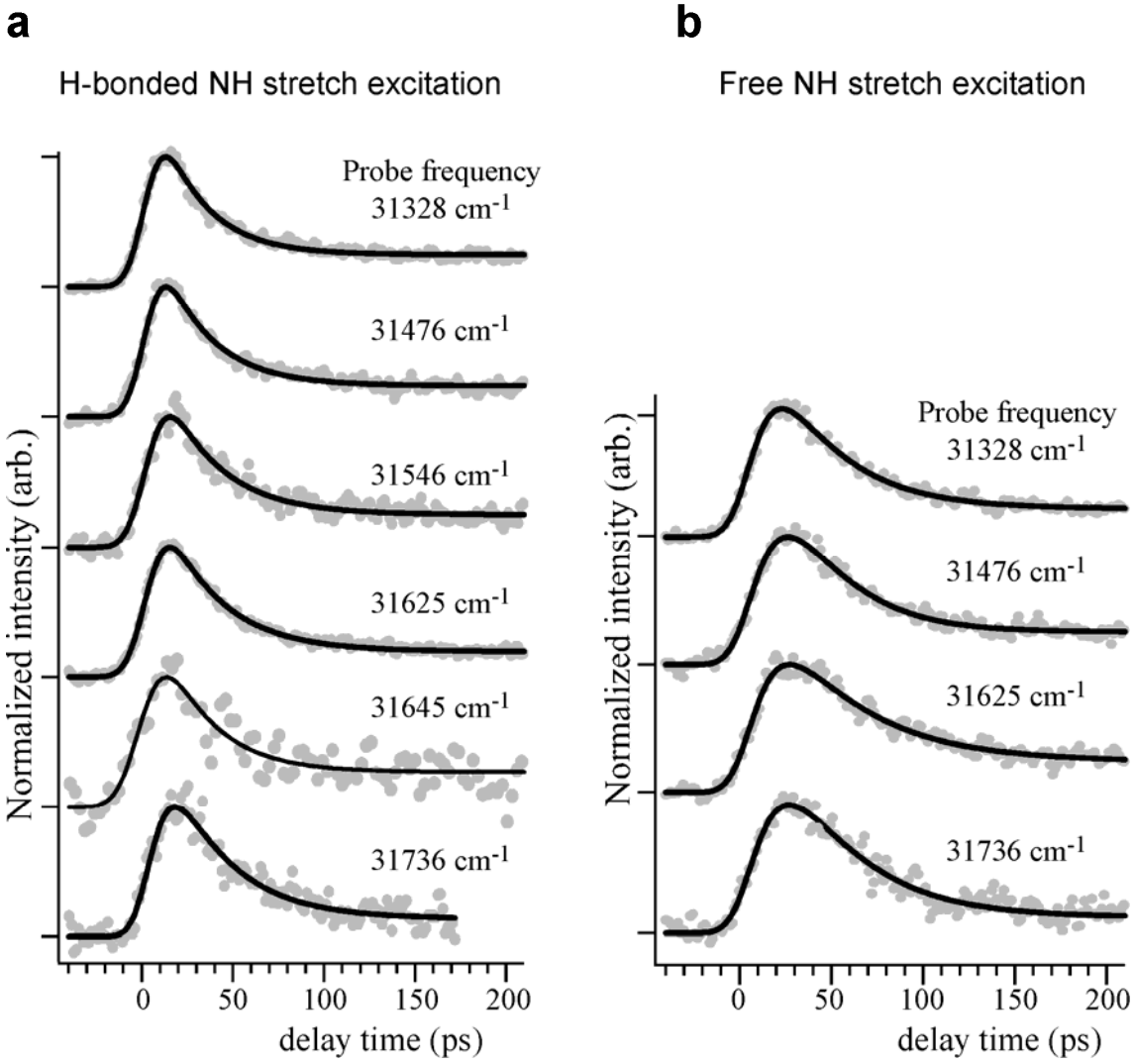

Fig. 7 Yamada et al.